International Journal of Advanced Smart Convergence Vol.13 No.2 103-109 (2024)
http://dx.doi.org/10.7236/IJASC.2024.13.2.103

IJASC 24-2-13

Strong Orientation Anchoring and Shear Flow of a Nematic Liquid Crystal

Won Hee HAN

Professor, Department of Railway Vehicle, Dong Yang University, YeungJu, Kyungbuk, Korea
whhan@dyu.ac.kr

Abstract

A nonlinear numerical analysis of orientation and velocity fields of the full Ericksen-Leslie theory for a nematic liquid crystal under shear flow is given. We obtained for the first time the three-dimensional orientation and two component velocity profiles evolutions for both in- and out-of-shear plane orientation anchorings. Complex evolution routes to steady state were found even for shear aligning nematic. As the Ericksen number increases monotonic evolution of velocity and orientation shifts towards multi-region nucleating director rotation growth with complex secondary flow generations. We found that contrary to the in-shear-plane anchorings like homeotropic or parallel anchorings, binormal anchoring gives rise to substantial non-planar three-dimensional orientation with nonzero secondary flow.

Keywords: *Nematic Liquid Crystal, Ericksen-Leslie Theory, Orientation Anchoring, Shear Flow, Frank Orientation Distortion Energy. Leslie Viscosity.*

1. INTRODUCTION

Liquid crystallinity is a distinct state of matter, simultaneously displaying both the long range molecular orientational order that gives rise to crystal-like properties (e.g., static birefringence, non-relaxing elasticity, etc.), and complete fluidity, of which various display technologies can take advantage [1]. Nematic liquid crystals have one-dimensional orientational order in which molecules tend to align towards a common unit vector called director [2]. The conservation laws for liquid crystal physics were given in [3]. The Frank orientation distortion energy equation was incorporated into viscous-orientational-elastic stress and couple stress expressions to build a continuum theory [4]. This theory is called Ericksen-Leslie (E-L) theory. While the E-L theory has been numerically solved for two-dimensional orientations during flow with only the in-shear-plane anchoring, it was not solved for three-dimensional orientation during flow with out-of-shear plane orientation anchoring [5-8]. The present study was able to numerically solve the three-dimensional orientation and two-component velocity profiles evolutions with both in- and out-of-shear plane orientation anchorings.

2. THEORY

The L-E theory consists of the following linear momentum conservation and the viscoelastic director torque balance equations with corresponding constitutive equations.

Manuscript Received: April. 21, 2024 / Revised: April. 30, 2024 / Accepted: May. 5, 2024
Corresponding Author: whhan@dyu.ac.kr
Tel: +82-54-630-1214, Fax: +82-54-630-1028
Author's affiliation (Professor, Department of Railway Vehicle, Dong Yang University, Korea)

$$\rho \frac{dv_i}{dt} = -\frac{\partial p}{\partial x_i} + \rho g_i + \frac{\partial}{\partial x_j}\sigma_{ji} \ , \tag{1}$$

$$\epsilon_{ipq} n_p \left(\gamma_1 N_q + \gamma_2 n_k A_{kq} - \frac{\partial F_d}{\partial n_q} + \frac{\partial}{\partial x_k} \frac{\partial F_d}{\partial \left(\frac{\partial n_q}{\partial x_k}\right)} \right) = 0 \ , \tag{2}$$

where ρ and p are density and pressure, respectively. v_i represents the *i-th* component of the velocity vector parallel to the x_i axis in cartesian coordinates; the usual right handed cartesian coordinates alternatively represent $x_1 = x,\ x_2 = y,\ x_3 = z$. (*d/dt*) means the material time derivative $(d/dt = \partial/\partial t + v_k \partial/\partial x_k)$. Here, Einstein summation convection for repeated indices is used like $(v_k \partial/\partial x_k = \sum_{k=1}^{3} v_k \partial/\partial x_k)$. g_i is the *i-th* component of gravity. σ_{ji} are the *i-th* components of the surface force per x_j-normal area having the unit of pressure. ϵ_{ipq} represents the alternating third order tensor. n_p represents the *p-th* component of the unit vector director representing local average molecular orientation. N_p represents *p-th* component of the director rotation rate vector with respect to the rotating background fluid. γ_1 and γ_2 are called rotational and irrotational viscosities, respectively. A_{kq} and ω_{kq} are the rate of deformation and rotation tensors, respectively. F_d is the Frank orientation curvature free energy per volume. And the corresponding constitutive equations are given below.

$$F_d = K_{11}\left(\partial n_p/\partial x_p\right)^2 + K_{22}\left(n_p \varepsilon_{prs} \partial n_s/\partial x_r\right)^2 + K_{33} \left| \varepsilon_{ijk}\, n_j \varepsilon_{krs} \partial n_s/\partial x_r \right|^2, \tag{3}$$

$$N_p = \partial n_p/\partial t + v_k \partial n_p/\partial x_k - \omega_{pk}\, n_k \ , \ 2\omega_{pk} = \frac{\partial v_p}{\partial x_k} - \frac{\partial v_k}{\partial x_p}, \ 2A_{pk} = \frac{\partial v_p}{\partial x_k} + \frac{\partial v_k}{\partial x_p} \ , \tag{4}$$

$$\sigma_{ji} = \frac{-\partial F_d}{\partial \left(\frac{\partial n_q}{\partial x_j}\right)} \frac{\partial n_q}{\partial x_i} + a_1 n_p n_q\, A_{pq}\, n_j n_i + a_2 n_j N_i + a_3 n_i N_j + a_4 A_{ji} + a_5 n_j n_p A_{pi} + a_6 n_i n_p A_{pj} \tag{5}$$

In addition to equation (1) and (2), the following constraints of continuity equation and unit length equation of director are solved together to obtain velocity vector, director vector and pressure in general.

$$\partial v_k/\partial x_k = 0 \ , \qquad n_p n_p - 1 = 0. \tag{6}$$

The present study uses adaptive torque balance equations to enhance computational stability and accuracy [9]. Orientation and flow coupling can be described with dimensionless numbers, which are the Ericksen number (E) and the Reynolds number (Re) defined as

$$E = (\alpha_3 - \alpha_2) HU/(K_{11}\, K_{22} K_{33}\,)^{1/3}, \qquad Re = \rho\, U\, H/(\alpha_4/2)\,, \tag{7}$$

where H and U mean gap thickness and upper plate speed, respectively. The Leslie viscosity α_4 is divided by two since the shear strain rate in the Ericksen-Leslie theory is a half of the usual Newtonian viscosity-stress relation. Ericksen number (E) represents a characteristic ratio between the viscous torque and the orientation elastic torque. Re is ignored since the biggest Re in this study is much less than 0.001.

3. COMPUTING SYSTEM

Figure 1(a) shows the shear flow geometry in which the shearing direction is along the x-axis and upper

plate starts moving at a constant speed of U at time *t=0* while the bottom plate is fixed. H is 350μm. Fig.1(b) shows three-dimensional director components $\mathrm{n}_x, \mathrm{n}_y, \mathrm{n}_z$. The length of the director is equal to one.

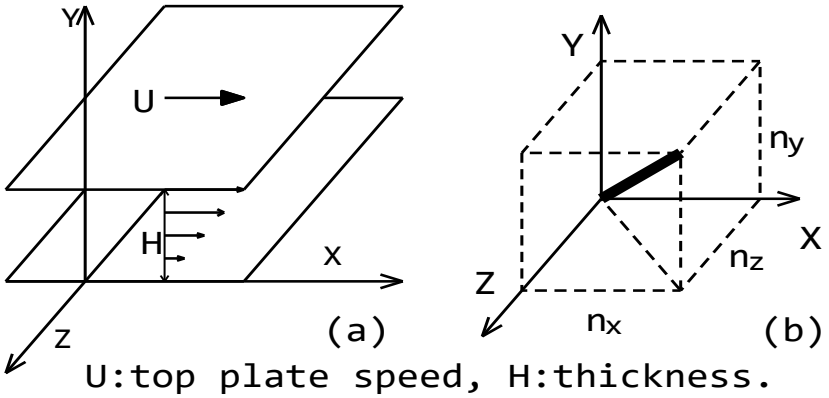

Figure 1. (a) Shear flow between two parallel plates and (b) director vector definition

The full governing equations are listed in [9], due to their long length they are not reproduced here. The five-component solution vector consists of the velocity field $(v_x(y,t),0,v_z(y,t))$ and the director field $(n_x(y,t),n_y(y,t),n_z(y,t))$ in y coordinate and time t. The x-directional velocity is called the primary velocity, and whenever $n_z \neq 0$, non-zero secondary velocity $(v_z \neq 0)$ parallel to the z-axis appears. The initial director orientation $\mathrm{n}_i^{\dagger}$ has been given a small but finite random perturbation mimicking real state as

$$n_i^{\dagger} = (n_i^* + \epsilon_i)/((n_k^* + \epsilon_k)(n_k^* + \epsilon_k))^{1/2}, \quad i = x, y, z, \tag{8}$$

where n_i^* represents the undisturbed initial orientation director field and ϵ_i the finite size (0.5 percent) random perturbation. At the bounding top and bottom surfaces two types of orientation anchoring conditions are considered. The first one is homeotropic anchoring for which the surface director is n_H=$(\mathrm{n_x} = 0, \mathrm{n_y} = 1, \mathrm{n_z} = 0)$, which is within x-y plane(in-shear plane). The second one uses surface director binormal to x- and y-axes, or out-of-shear plane, denoted as n_B=$(n_x = 0, n_y = 0, n_z = 1)$. The Leslie anisotropic viscosities and Frank orientation distortion constants in the E-L theory used in this paper are shown in Table 1 [9].

Table 1. Ericksen-Leslie continuum theory constants

Leslie Viscosities	α_1	α_2	α_3	α_4	α_5	α_6
Unit(Pascal*s)	-0.0203	-0.406	-0.0376	0.490	0.329	-0.116
Frank Elasticity	K_{11}(Splay mode)		K_{22}(Twist mode)		K_{33}(Bend mode)	
Unit(10^{-11}Newton)	0.67		0.37		0.77	

The computational method uses Galerkin finite elements to discretize space and finite difference to discretize time. The gap thickness coordinate (y) is discretized into 100 linear elements and the time (t) discretization is carried out by a fully implicit Euler method. Newton-Raphson method was used to compute the resulting equation set [9]. Exact Jacobian equations and their Fortran conversions were obtained with two open source computer algebra systems [10, 11].

4. RESULTS AND DISCUSSION

Figure 2 shows evolutions of velocity and director profile along the dimensionless thickness coordinate ($y^* = y/H$) for E=6.5 and n_H. Fig.2(a) shows dimensionless primary velocity ($v_x^* = v_x/U$) profile as functions of y^* evolving from curvy to less curvy Newtonian-like profile with increasing nominal strains ($\gamma = t \cdot U/H$) indicated in the legend. Fig.2(b) shows the corresponding dimensionless secondary velocity ($v_z^* = v_z/U$) profile evolution, which shows an initial growth followed by rapid decay. Fig.2(c) shows x-component of director n_x profile evolution indicating that n_x grows fastest in the center. This evolution direction is towards the lowest Miesowicz viscosity director orientation [2]. Fig.2(d) shows y-component of director n_y which corresponds to escape from the highest Miesowicz viscosity director orientation. Fig.2(e) shows vanishing z-component of director n_z profiles indicating stability of in-shear-plane orientation.

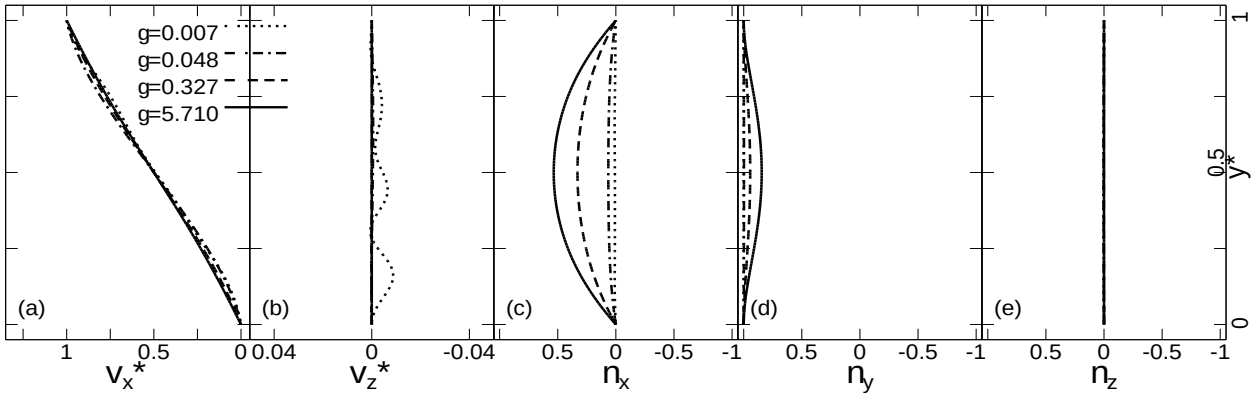

Figure 2. Evolutions of dimensionless velocities and director profiles for E=6.5 and n_H

Figure 3 shows steady state velocity and director orientation for different E values indicated in the legend for n_H. Fig.3(a) shows v_x^* profile which becomes more Newtonian-like with increasing E. Fig.3(b) shows vanishing v_z^* profile at steady state indicating that in-shear-plane solution is stable. Fig.3(c) shows x-component of director approaching a limiting value with increasing E, which occurs throughout the whole y^* space except near the boundary. Fig.3(d) shows y-component of director also approaching a limiting value within the in-shear-plane with increasing E. Fig.3(e) shows vanishing z-component of director indicating stability of in-shear-plane orientation as the initial orientation perturbation decays.

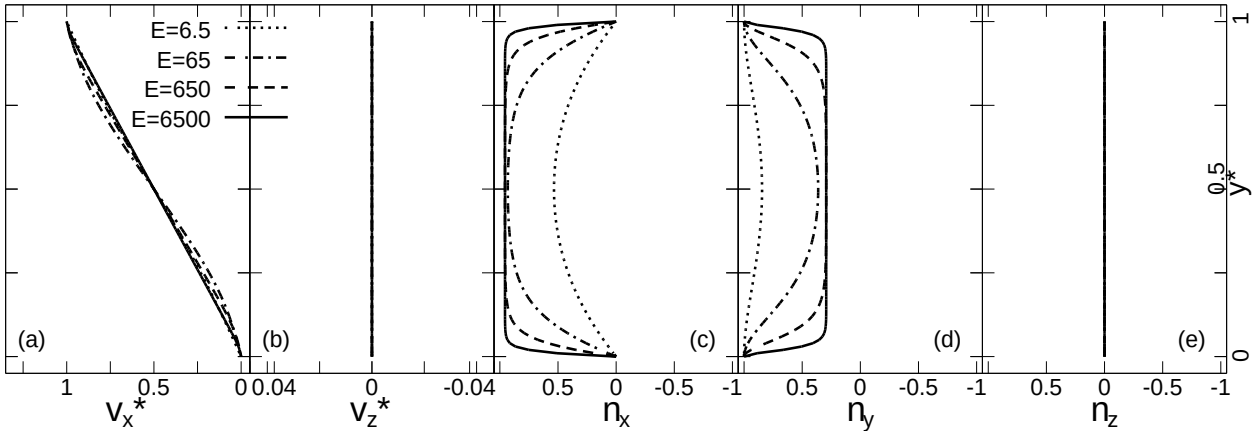

Figure 3. Steady state dimensionless velocities and director profiles for n_H

As E increases, vanishing viscous torque condition at Leslie angle θ_a is met as shown below [4].

$$\tan\theta_a = ((\lambda\text{-}1)/(\lambda\text{-}1))^{1/2}, \quad \lambda = -\gamma_2/\gamma_1,\ \gamma_1 = \alpha_3 - \alpha_2\ ,\ \gamma_2 = \alpha_6 - \alpha_5,\ \mathrm{Cos}\theta_a = n_x = 0.956 \qquad (9)$$

Equation (9) is valid when $n_z = 0$. When the orientation anchoring is binormal to both the homeotropic orientation and shearing direction, above some critical Ericksen number, the director starts escaping from the x-z orientation plane, and rotates towards the shear plane which are spanned by the x- and y- axes as shown in Figure 4 for E=32.7. Fig.4(a) shows nearly Newtonian-like v_x^* profile throughout the whole evolution with increasing γ as indicated in the legend. However, fig.4(b) shows a corresponding substantial nonvanishing v_z^* profile evolution. The initial director orientation is within the x-z plane throughout y-space. Fig.4(c) shows director escape towards the x-axis, which is faster than the director escape towards the y-axis as shown in fig.4(d). The director escaping process is also shown in decreasing z-component of director profile evolution shown in fig.4(e), which reaches steady state before the strain value of 101. The central region director escapes fastest. However, n_z does not vanish, and neither does the dimensionless secondary velocity at steady state.

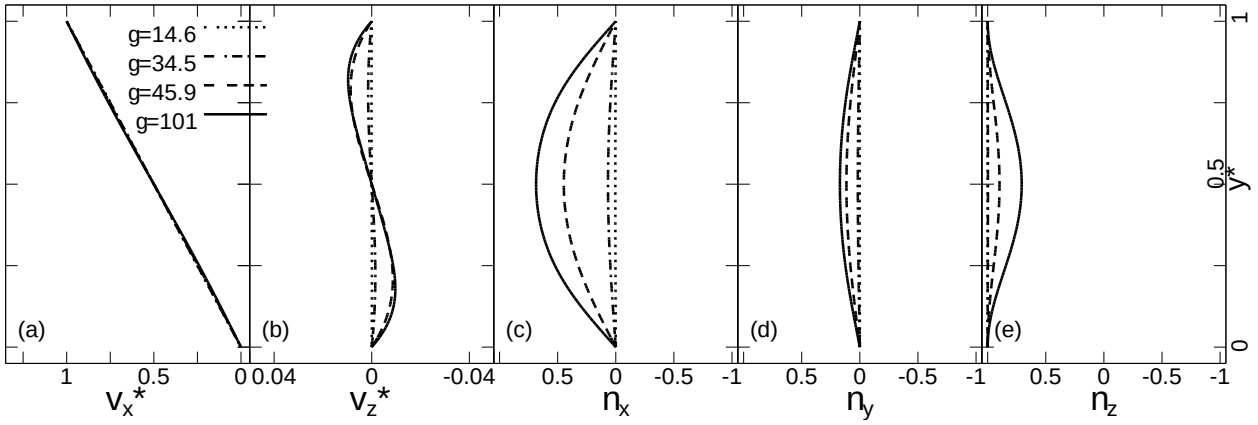

Figure 4. Evolutions of dimensionless velocities and director profiles for E=32.7 and n_B

If $n_z \neq 0$, there will be secondary flow along the z-axis although its magnitude is relatively smaller than the magnitude of the x-directional primary velocity. At E=32.7 director could not reach the Leslie angle yet due to the resisting Frank elastic director torque. As the Ericksen number further increases, a new phenomenon is observed. Figure 5 shows a complex v_x^*, v_z^* and three-dimensional director n_x, n_y, n_z profile evolutions throughout y^* space for E=1309. Fig.5(a) shows Newtonian-like v_x^* profile which remains more or less the same throughout the whole evolution while (b) shows complex wave-like evolution of v_z^* profile strongly coupled with the three-dimensional orientation profile shown in fig.5(c-e). Instead of director escape occurring primarily in the center, director escape occurs in multiple regions and the escape growth direction signs are not all the same. Director escape from x-z plane occurs towards both plus and minus direction, but single sign growth eventually dominates to reach the Leslie angle where viscous torque vanishes.

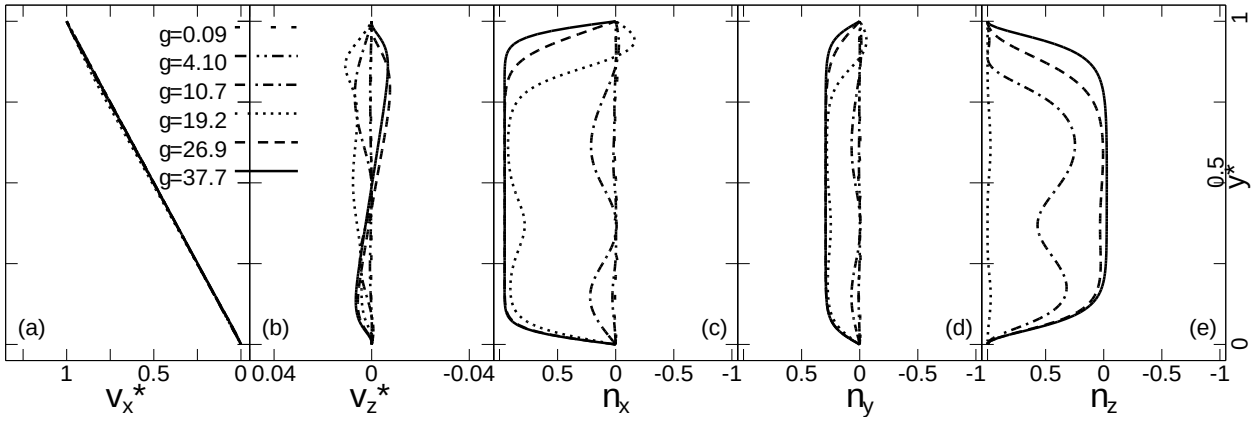

Figure 5. Evolutions of dimensionless velocities and director profiles for E=1309 and n_B

Figure 6 shows steady state orientation and velocity fields with binormal anchoring for a series of Ericksen numbers. Fig.6(a) shows almost like Newtonian v_x^* profile, but substantial amount of nonzero v_z^* can be seen with opposite signs at lower and upper half y^* coordinate region in fig.6(b). Fig.6(c) shows x-component of director reaching the Leslie angle equivalent shown in equation (9) in the center region. Fig.6(d) shows y-component of director also monotonically reaching the Leslie angle equivalent for $n_y = sin\theta_a$ with increasing E when $n_z = 0$. Fig.6(e) shows z-component of director also monotonically reaching $n_z = 0$ line in the center region that does not hint any complex nature of multiple routes to the steady state. Although the dimensionless primary velocity and the three-dimensional director profile show monotonic variation with increasing E values, the dimensionless secondary velocity v_z^* profile does not decay and even changes its pattern with increasing E.

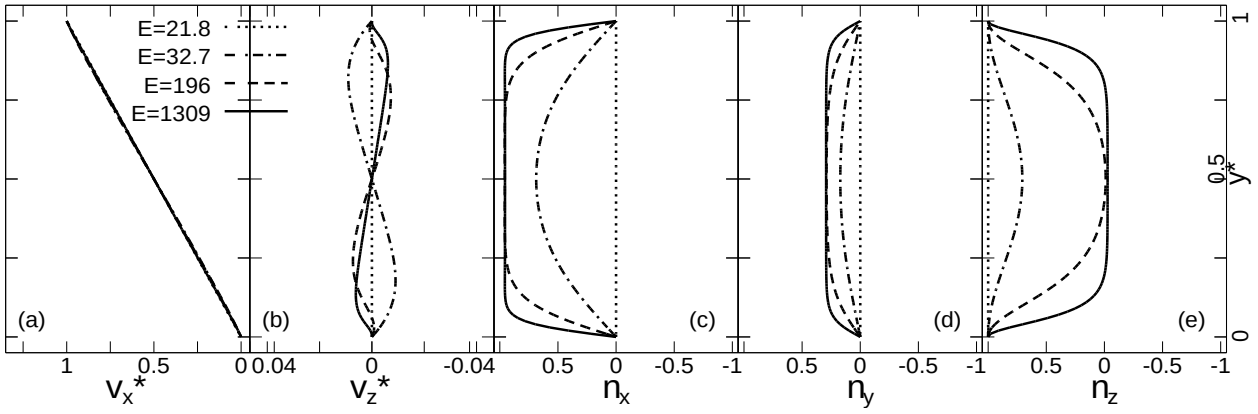

Figure 6. Steady state dimensionless velocities and director profiles for n_B

5. CONCLUSION

The homeotropic anchoring showed orientation evolution within the shear-plane during shear flow monotonically reaching the vanishing viscous torque condition of equation (9) in most part of the computation domain. However, binormal anchoring, which represents surface director anchoring normal both to the shearing direction and homeotropic axis, gave a nonvanishing secondary flow and nonplanar three-dimensional orientation even at steady state. Although the center region for higher Ericksen number eventually accommodates the vanishing viscous torque condition, the routes towards the vanishing viscous torque get

more complex as the Ericksen number increases. This study revealed multi-region nucleating director escapes at higher Ericksen number with binormal anchoring that also proved the versatility of the adaptive torque balance equations. If two- or -three-dimensional gradients are considered, experimentally observed roll patterns and other orientation structures may emerge. We showed that increasing the Ericksen number not just enforces vanishing viscous torque condition but also brings more complex transient evolution patterns due to the viscoelastic torque balance coupled with the linear momentum balance of the full L-E theory. The possibility of weak anchoring with three-dimensional orientation considering both surface energy and surface viscous torque instead of strong anchoring will be explored in the next study.

References

[1] C. Jang, "A study on development of VR-based tangible functional game for prevention of dementia," *International Journal of Advanced Culture Technology (IJACT)*, Vol.9, No.1, pp. 196-202, 2021.
DOI: https://doi.org/10.17703/IJACT.2021.9.1.196

[2] P. G. De Gennes, and J. Prost, *The physics of liquid crystals*, Oxford university press, pp. 99, 1993.

[3] J. L. Ericksen, "Conservation laws for liquid crystals," *Transactions of Society of Rheology*, Vol. 5 pp 23-34, 1961.
DOI: https://doi.org/10.1122/1.548883

[4] F. M. Leslie, "Some constitutive equations for liquid crystals," *Archive for Rational Mechanics and Analysis*, Vol. 28, pp. 265–283, 1968.
DOI: https://doi.org/10.1007/BF00251810

[5] P. J. Barratt, and I. Zuniga, "A theoretical investigation of the Pieranski-Guyon instability in Couette flow of nematic liquid crystals," *Journal of Non-Newtonian Fluid Mechanics*, Vol.11, pp23-36, 1982.
DOI: https://doi.org/10.1016/0377-0257(82)85013-1

[6] L. R. P. de Andrade Lima, and A. D. Rey, "Poiseuille flow of Leslie-Ericksen discotic liquid crystals: solution multiplicity, multistability, and non-Newtonian rheology," *Journal of Non-Newtonian Fluid Mechanics*, Vol.110, pp. 103-142, 2003.
DOI: https://doi.org/10.1016/S0377-0257(03)00006-5

[7] K. Fedorowicz, and R. Prosser, "On the simulation of nematic liquid crystalline flows in a 4:1 planar contraction using the Leslie-Ericksen and Beris-Edwards models," *Journal of Non-Newtonian Fluid Mechanics*, Vol. 310, 104949, 2022.
DOI: https://doi.org/10.1016/j.jnnfm.2022.104949

[8] J. R. L. Cousins, S. K. Wilson, N. J. Mottram, D. Wilkes, and L. Weegels, "Squeezing a drop of nematic liquid crystal with strong elasticity effects," *Physics of Fluids*, Vol. 31, No. 8, 083107, August 2019.
DOI: https://doi.org/10.1063/1.5110878

[9] W. H. Han, *Computational Modelling of Orientation and Flow Instabilities, Textures, Rheology, and Optics of Shearing Nematic Liquid Crystalline Materials*, Ph.D. Thesis. McGill University, Montreal, CANADA, 1995.

[10] Yet Another Computer Algebra System, YACAS, *http://yacas.org*

[11] Maxima, A Computer Algebra System, *https://maxima.sourceforge.io*